Energy Reports 9 (2023) 448–453

Contents lists available at ScienceDirect

Energy Reports

journal homepage: www.elsevier.com/locate/egyr

Solid-state transformer modelling in power flow calculation☆

Zahid Javid [a,*], Ulas Karaagac [a], Ilhan Kocar [a], William Holderbaum [b]

[a] Department of Electrical Engineering, The Hong Kong Polytechnic University, Hung Hom, Kowloon, Hong Kong, China
[b] School of Engineering, Manchester Metropolitan University, John Dalton Building, Chester Street, M15GD Manchester, United Kingdom

ARTICLE INFO

Keywords:
Modified augmented nodal analysis
Newton Raphson algorithm
Power flow
Solid-state transformer

ABSTRACT

This article proposes a novel Solid-State Transformer (SST) power flow (PF) model which is implemented with Modified Augmented Nodal Analysis (MANA) formulation using Newton-Raphson (NR) algorithm. Any network topology can be handled by the MANA formulation, and it can be easily and methodically expanded to include other components, like SST. Since various types of buses can have various type converters and SSTs, the sum of line flows are used instead of classical bus power injections equations. The proposed approach is coded in MATLAB and tested on an IEEE 33 bus distribution test feeder. The results are compared with Holomorphic Embedding PF method (HE-PFM) and with existing methodology in literature. In line with the findings, the proposed approach achieves accurate representation of SST, better convergence characteristics with a faster simulation speed compared to HE-PFM.

1. Introduction

The solid-state transformer (SST) is a device that can provide power quality solutions for smart grids applications (Mishra, 2021). McMurray initially suggested the notion of SST in 1968, proposing a solid-state device with high frequency isolation that acts like a low frequency conventional transformer (Mcmurray, 1970). SST found practical application in traction systems in the 1990 s, when weight and volume reduction were critical, because the standard solution was based on a low frequency transformer, resulting in a huge and heavy system. The use of mechanical actuators or tap changers will no longer be needed, thanks to ability of SST to compensate for voltage sags, linking asynchronous networks, interface DC and AC port(s), compensate reactive power, regulate voltage magnitude, isolate disturbances from the source and load, and vice versa. In a conventional distribution network (DN) the low voltage DC (LVDC) and medium voltage DC (MVDC) buses links DC units like photovoltaic (PV), energy storage systems (ESSs), and DC loads to the LVDC bus. The DC units must be connected to the MVDC grid using two power conversion stages in these conditions since galvanic isolation is not maintained. More converters are thus needed, which boosts the overall cost. In reference (Zhuang, 2021) a novel multiport DC SST (M-DC-SST) was proposed as a direct interface between the DC units and the MVDC bus. The DC units are connected separately on the LV side, while different modules are connected on the MV side in series. To save money and reduce the number of converters, in contrast to a normal DC DN, authors connected the DC units to the MVDC bus without using an extra converter or an LVDC bus. One of the emerging technologies, SST, will be extensively utilized in the future to combine LV and MV networks with control circuits and power electronics converters, making it easier to include renewable energy sources in smart grid applications (Mollik, 2022).

The demand on LV networks will increase as heating and transportation become more electrified, which might lead to overburdened MV/LV transformers and LV cables. The LVDC DNs and the installation of SSTs at MV/LV substations can solve these problems. Although the SST offers several benefits over the traditional transformer, it also presents certain operating difficulties. For example, while SST produces low fault currents and is generally employed in LV networks, its restricted short-circuit capabilities can drastically affect the behavior and needs for LV fault deterrence. Accurate SST modelling in power flow (PF) calculation is another challenge. The SST model in OpenDSS (Guerra and Martinez-Velasco, 2017) is case specific and offers limited SST control options. A planning approach based on particle swarm optimization (PSO) was presented for optimally locating and sizing SST installations with the objective of reducing radial distribution network losses in (Syed et al., 2018). The research also investigated various reactive power support schemes of SST. The PF solution in (Guerra and Martinez-Velasco, 2017) is based on backward-forward-sweep (BFS)

☆ 2023 8th International Conference on Sustainable and Renewable Energy Engineering (ICSREE 2023), 11-13 May, Nice, France.

* Corresponding author.
E-mail address: zahid.javid@connect.polyu.hk (Z. Javid).

https://doi.org/10.1016/j.egyr.2023.12.003
Received 31 October 2023; Accepted 1 December 2023
Available online 8 December 2023

method. However, the BFS approach lacks generality and has topological restrictions (Kocar et al., 2013). The inclusion of the Modified Augmented Nodal Analysis (MANA) significantly enhances the field of electrical circuit theory and analysis (Wedepohl and Jackson, 2002). The MANA formulation was explored in literature for PF studies due to its flexibility to model any arbitrary device with arbitrary constraints (Kocar et al., 2013; Nduka et al., 2019; Cetindag et al., 2017). As MANA formulation is superior to the traditional nodal analysis formulation (Javid et al., 2023), SST model is developed for this formulation in addition to the Holomorphic Embedding PF method (HE-PFM) (Trias, 2012). The HE-PFM is a novel PF solution that handles PF problems in order to approximate the bus voltage rationally (Ra o et al., 2015).

The representation of losses is a facet of the SST that needs special consideration. An SST model that can estimate the SST losses for all operating scenarios is a topic under research which needs further investigation. The SST losses mainly depend on the SST configuration and its switching strategy. Consequently, the objective of this study is to propose a general SST PF model with MANA formulation that could reflect any SST configuration.

The remaining paper is structured as follows. The SST model is developed in Section 2. MANA formulation is presented in Section 3. Section 4 contains simulation results and discussions. The conclusions are made in Section 5.

2. SST model overview and line flow equations

The commonly used three-stage SST detailed model is shown in Fig. 1, while Fig. 2 shows the simplified models of different SSTs. Table 1 gives an overview of the converter ratings and functionalities of each stage. It is notable that the ratings of the various SST stages are determined by the amount of power they can handle. For instance, stage 3 must be rated appropriately since it supports the entire load apparent power. Stages 1 and 2 can be rated lower than stage 3 since they only support the load active power.

2.1. SST model

To derive the formulation, consider the connections of three stage SST between buses shown in Fig. 3. The first two topologies in Fig. 2 can easily be extracted from the presented formulation. Our objective is to calculate the total power injection at sending bus.

The voltage and power relationships between different stages are given below.

Stage 1:

$$V_j = \varsigma_1 M_1^{-1} V_{i,LL_{rms}} \tag{1}$$

where, M_1: modulation index (of stage 1 converter); and ς_1: converter constant (of stage 1 converter)

$$V_{base}^{mvdc} = \varsigma_1 V_{base}^{mvac} \tag{2}$$

If we assume bases selection as given in (2), then, $V_{ac}^{pu} = V_{dc}^{pu}$ at $M_1 = 1$. The relationship between output/input powers of stage 1 can be written follows.

$$P_i = \eta 1^{-1} P_j \tag{3}$$

Stage 2:

$$V_k = DV_j \tag{4}$$

where, D is the duty cycle ratio.

$$P_j = \eta 2^{-1} P_k \tag{5}$$

Stage 3:

$$V_{m,LL_{rms}} = \varsigma_3 M_3^{-1} V_k \tag{6}$$

where, M_3: modulation index; ς_3: converter constant of stage 3 converter.

$$V_{base}^{lvdc} = \varsigma_3 V_{base}^{lvac} \tag{7}$$

Similarly, as in stage 1, for given base selection in (7) $V_{ac}^{pu} = V_{dc}^{pu}$ at $M_3 = 1$. The relationship between output and input power depends on inverter efficiency, as given below.

$$P_k = \eta_3 P_m \tag{8}$$

2.2. Line flows with SST connection

To find a PF solution our objective is to calculate the total power injection at each bus. Due to multiple SST connections between buses, line flows are summed up instead of conventional power injection equation. The total power injection at bus "i" in Fig. 3 is given below.

$$P_i = P_{ia} + P_{ib} + P_{ic} \tag{9}$$

$$P_{ia} = \frac{Y_{ma}\,\eta_3}{\eta_1\,\eta_2}\left(M_3^2 V_{m,pu}^2 - M_3 V_{m,pu} V_{a,pu}\right) \tag{10}$$

$$P_{ib} = \frac{Y_{kb}}{\eta_1\,\eta_2}\left(D^2 V_{k,pu}^2 - DV_{k,pu} V_{b,pu}\right) \tag{11}$$

$$P_{ia} = \frac{Y_{jc}}{\eta_1}\left(M_1^{-2} V_{j,pu}^2 - M_1^{-1} V_{j,pu} V_{c,pu}\right) \tag{12}$$

$$\eta_{SST} = \eta_3/\eta_1\eta_2 \tag{13}$$

where, η_{SST} is the overall SST efficiency.

The expressions (1−12) are derived for load model of SST and can be modified easily for generation mode as explained below.

2.3. Load and generation modes

As seen in Fig. 2, the SST acts as a two-terminal device. The secondary LV side of stage 3 provides both active power (P) and reactive power (Q) to the LV loads while keeping the secondary terminal voltage

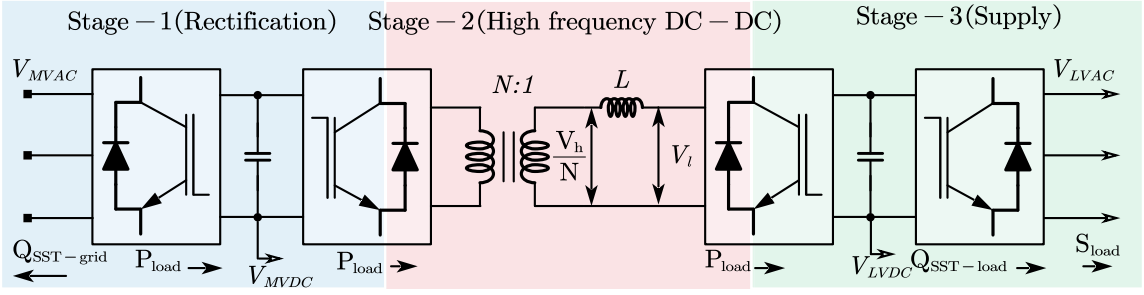

Fig. 1. General three-stage SST model.

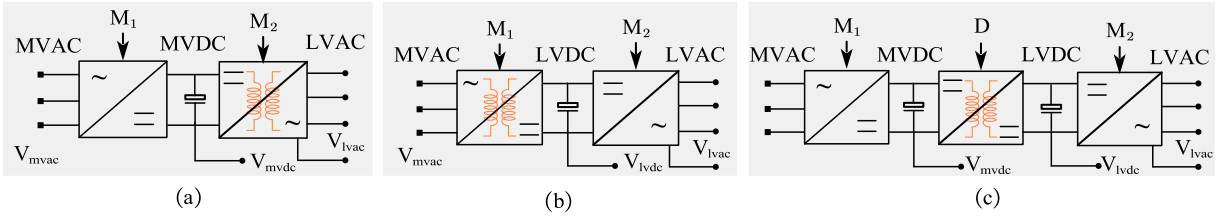

Fig. 2. Simplified SST models: (a) 2-stage SST model with MV DC-link; (b) 2-stage SST model with LV DC-link; (c) 3-stage SST model with MV and LV DC-links.

Table 1
SST functionalities and rating overview.

Stage	Function	Input	Output	Rating
1	Controlled rectification	MVAC	MVDC	$\sqrt{P_{load}^2 + Q_{SST-Grid}^2}$
2	DC-DC conversion	MVDC	LVDC	P_{load}
3	Load supply voltage	LVDC	LVAC	S_{load}

constant (for example, at 1 p. u.). The SST requires only active power from the primary MV side. Due to the dual directionality of the SST, there are two distinct operating modes: load and generation modes (see Fig. 4).

The followings are the fundamental relationships between the active powers on each side of the SST in different modes of operation.

$$P_p = P_{s/\eta_{SST}} \;;\; Q_p = 0 \quad \text{Load mode} \tag{14}$$

$$P_p = \eta_{SST} P_s \;;\; Q_p = 0 \quad \text{Generation mode} \tag{15}$$

where, subscripts p and s are primary (MV) and secondary (LV) terminals of the SST.

The efficiency curve for SST used in this research is based on the results presented in (Guerra and Martinez-Velasco, 2017; Qin and Kimball, 2010). Since load power factor (pf) has an influence on SST efficiency, the following strategy has been employed.

$$\eta\,(\psi,\ \text{pf}) \ = f(\psi) \times \beta\,(\text{pf}) \tag{16}$$

where, η efficiency for a load level (ψ) at a power factor (pf); $f(\psi)$: function of load at unity pf ($\psi = KVA/KVA_{rated}$), and β is the scaling factor which depends on the pf.

In this study we used the following approach and it valid for $\psi > 5\%$, see (Qin and Kimball, 2010).

$$\beta(\text{pf}) \ = \ 0.98 + 0.02\text{pf} \tag{17}$$

3. MANA formulation

The readers are directed to for an elementary introduction to MANA method for PF applications (Wedepohl and Jackson, 2002; Javid et al., 2023a; Javid et al., 2023b). The current of Non-Constitutive Elements (NCE) are included as state variable in the MANA formulation in addition to the voltages. These network components (NCEs) have current expressions that are difficult to express as a function of their terminal voltages alone. The MANA formulation can be summarized as follows.

$$F(u) = \left[Y_{Aug}\right]\ u + I_{PQ} - I_{\ gen} - H \tag{18}$$

where u: vector of state variables; I_{PQ}: augmented vector for non-linear loads; I_{gen}: augmented vector of currents for generator nodes; and H: vector of independent sources (voltage and currents). Y_{aug} can be form as follows.

$$\left[Y_{aug}\right] = \begin{bmatrix} Y & A_1 \\ A_2 & A_3 \end{bmatrix} \tag{19}$$

where Y: system admittance matrix; A_1, A_2, and A_3 are the block matrices (network elements that are hard to express with admittance model).

In (18) the slack bus characterized as voltage source. Similar to classical nodal analysis (CNA), the linear loads are integrated directly

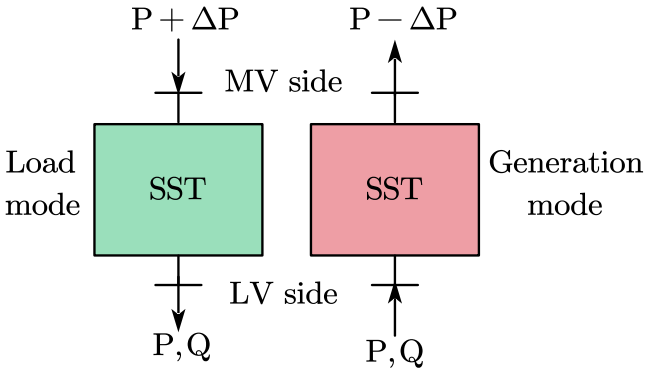

Fig. 4. Load and generation modes of SST.

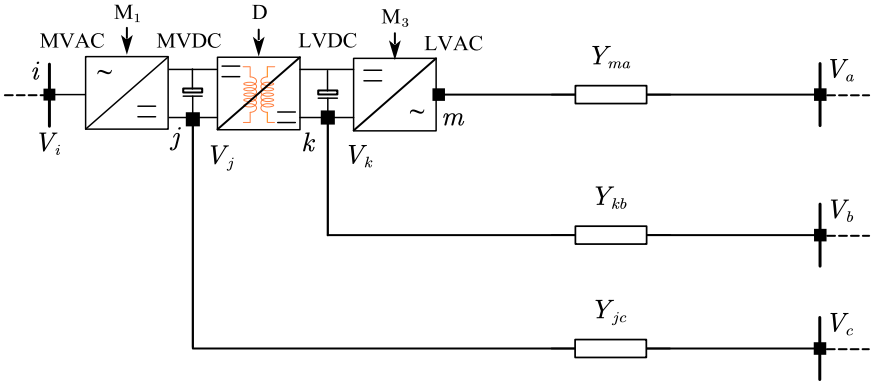

Fig. 3. SST connection in a hybrid AC/DC DN.

into Y matrix (Wedepohl and Jackson, 2002). The solution of Eq. (12) requires the use of an iterative approach due to the existence of non-linear (PQ) loads. To resolve this, we use the Newton Raphson (NR) technique.

$$\Delta u^{(t)} = -\left[(J)^{(t)}\right]^{-1} F(u)^{(t)} \tag{20}$$

$$u^{(t+1)} = (u)^{(t)} + (\Delta u)^{(t)} \tag{21}$$

where, J: Jacobian matrix; and t: iteration counter.

SST integration into grid creates a hybrid AC/DC network configuration. To generalize the suggested modeling approach to fit diverse network designs, it is advantageous to integrate certain practical aspects.

B = Buses.

C_{ij}: System connectivity matrix (Javid et al., 2022).

W: Binary vector to define type of bus (AC or DC).

L: Binary vector to define type of Line (AC or DC).

Note that the binary value for ac is false (zero) and for dc its true (one).

A generic expression for the specified powers at bus "i" can be derived as follows.$P_i^{sp} = \overline{W}_i(P_i^{g,ac} - P_i^{l,ac} + \eta_{i,inv}P_i^{g,dc} - \eta_{i,rec}^{-1}P_i^{l,dc}) + W_i(P_i^{g,dc} - P_i^{l,dc} - \eta_{i,rec}P_i^{g,ac} - \eta_{i,inv}^{-1}P_i^{l,ac}), \quad \forall i \in B$ (22)

$$Q_i^{sp} = \overline{W}_i\left(Q_i^{g,ac} - Q_i^{l,ac} + Q_{i,conv}^{g,dc} - Q_{i,conv}^{l,dc}\right) + W_i \times 0 \tag{23}$$

where, *sp*: specified; *g*: generation; *l*: load; *conv*: converter *rec*: rectifier, *inv:* inverter.

It is essential to note that the bar above the binary variables denotes the complement of the binary element.

Below are the equations that express the constraints for active and reactive loads.

$$F_l(l_p) = P_i^{(t)} - re\left(I_l^* V_l\right)^{(t)} \tag{24}$$

$$F_l(l_q) = Q_i^{(t)} - im\left(I_l^* V_l\right)^{(t)} \tag{25}$$

where, l_p and l_q are the indices for P and Q loads respectively; I_l: load current; V_l: load voltage; and $P_i^{(t)}$, and $Q_i^{(t)}$, are the real and reactive power of i^{th} load at t^{th} iteration as shown below in (26) and (27).

$$P_i^{(t)} = P^{sp}\left(\left|V_l^{(t)}\right| / V^{sp}\right)^{n_p} \tag{26}$$

$$Q_i^{(t)} = Q^{sp}\left(\left|V_l^{(t)}\right| / V^{sp}\right)^{n_q} \tag{27}$$

where, n_p and n_q are constants to define the type of load, i.e., for a constant power load (CPL)→ $n_p = n_q = 0$; for a constant current load (CCL)→ $n_p = n_q = 1$; and for a for constant impedance load→ (CIL) $n_p = n_q = 2$.

The calculated active power and reactive power at the sending bus "i" can be expressed generally as follows.$P_i^{cal} = \sum_{\substack{j=1 \\ j\neq i}}^{B} [C_{ij}][\overline{W}_i\overline{L}_{ij}\overline{W}_j[P_{ij}] + \overline{W}_iL_{ij}\overline{W}_j[P_{ij}] + \overline{W}_iL_{ij}W_j[P_{ij}] + W_iL_{ij}\overline{W}_j[P_{ij}] + W_iL_{ij}W_j[P_{ij}]]$ (28)

$$Q_i^{cal} = \sum_{\substack{j=1 \\ j\neq i}}^{B} [C_{ij}]\left[\overline{W}_i\overline{L}_{ij}\overline{W}_j[Q_{ij}] + \overline{W}_iL_{ij}\overline{W}_j[P_{ij}](\tan\varphi_c) + \overline{W}_iL_{ij}W_j[P_{ij}](\tan\varphi_c)\right] \tag{29}$$

where, ϕ_c is converter power factor angle.

The current of both the CPL and CCL loads is regarded as an independent variable in the MANA formulation. Following is a general formulation for the Jacobian entries that can be used with any type of load:$\partial F_l(l_p)/\partial V_{l,re} = \frac{n_p \times P^{sp} \times V_{l,re} \times (V_{l,im}^2 + V_{l,re}^2)^{\frac{n_p}{2}-1}}{(V^{sp})^{n_p}} - I_{l,re}$ (30)

$$\partial F_l(l_p)/\partial V_{l,im} = \frac{n_p \times P^{sp} \times V_{l,im} \times \left(V_{l,im}^2 + V_{l,re}^2\right)^{\frac{n_p}{2}-1}}{(V^{sp})^{n_p}} - I_{l,im} \tag{31}$$

$$\partial F_l(l_p)/\partial I_{l,re} = -V_{l,re} \tag{32}$$

$$\partial F_l(l_p)/\partial I_{l,im} = -V_{l,im} \tag{33}$$

$$\partial F_l(l_q)/\partial V_{l,re} = \frac{n_q \times Q^{sp} \times V_{l,re} \times \left(V_{l,im}^2 + V_{l,re}^2\right)^{\frac{n_q}{2}-1}}{(V^{sp})^{n_q}} + I_{l,im} \tag{34}$$

$$\partial F_l(L_q)/\partial V_{l,im} = \frac{n_q \times Q^{sp} \times V_{l,im} \times \left(V_{l,im}^2 + V_{L,re}^2\right)^{\frac{n_q}{2}-1}}{(V^{sp})^{n_q}} - I_{l,re} \tag{35}$$

$$\partial F_l(l_q)/\partial I_{l,re} = -V_{l,im} \tag{36}$$

$$\partial F_l(L_q)/\partial I_{l,im} = V_{l,re} \tag{37}$$

The mismatch vector is given below.

$$F(u) = \begin{cases} P_i^{sp} - Pi^{cal} & , \quad \forall i \in B \\ Q_i^{sp} - Qi^{cal} & , \quad \forall i \in B \end{cases} \tag{38}$$

4. Results and discussion

To verify the accuracy of the proposed method, we utilize IEEE 33-bus DN, depicted in Fig. 5. The test network data is taken from (Syed et al., 2018). The accuracy of the proposed approach is assessed and contrasted with the Holomorphic Embedding PF method (HE-PFM) and with reference (Syed et al., 2018). Authors are referred to (Trias, 2012; Ra o et al., 2015) for details of HE-PFM. The simulations were performed on a desktop PC with the following specs using MATLAB 2022b: RAM = 16 GB Processor = Intel Core i7 (3.21 and 3.19 GHz).

There may be a variety of options available to utilities for integrating SST into their distribution networks. In this study, SST is estimated to provide around 10% of the system's load. In the case of the 33-bus DN, the specified rating for the single SST is fixed at 150 kVA, while the overall load is set at 500 kVA. The DN is divided into four zones, as illustrated in Fig. 5. There are two scenarios in which the utility may decide to either split the installations into smaller units or create a single large SST with a high rating. Two simulation scenarios were considered for this study. First is the base case when there is no SST, and in second case SSTs are placed at different locations, with one SST in each zone. A fixed total load of 500 kVA is supplied through the SST. The voltage profiles of the test feeder are illustrated in Fig. 6, while Fig. 7 shows the variation in losses with increased Q injection from SST. The network's base case losses amount to 202.67 kW.

Table 2 shows the results of four SSTs at the locations shown in Fig. 5. Table 3 compares the results for network losses with multiple SSTs in the network. The locations of the SSTs and their ratings are also shown in Table 2 and Table 3. Table 3 demonstrates that as penetrations of SSTs

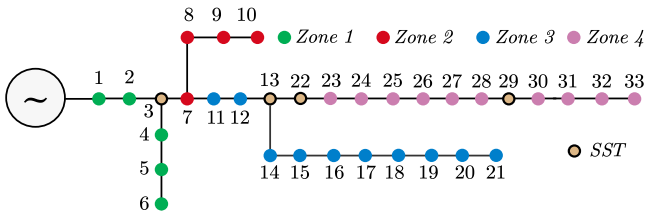

Fig. 5. IEEE 33-bus DN with SST locations.

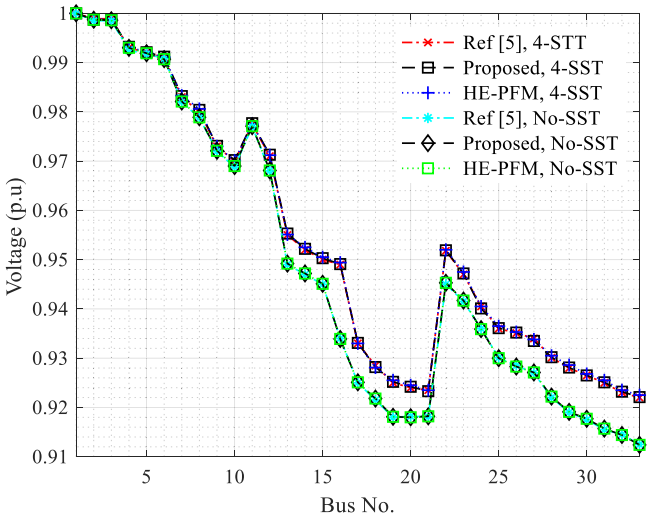

Fig. 6. Voltage profile.

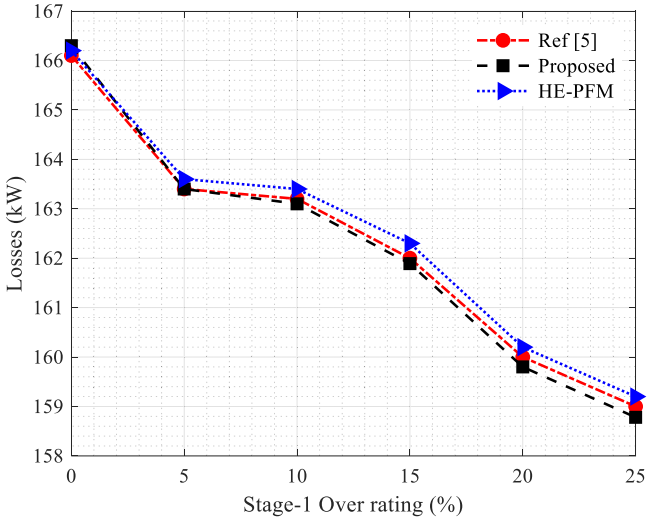

Fig. 7. Losses as a function of reactive power injection of SST.

increase, their benefits become more apparent. To comprehend the trend in losses as penetrations of SSTs, initially, just one SST of 500 kVA was considered at node 29. From this point forward, 100 kVA SSTs are added in the system. The optimal location of SSTs was obtained from reference (Syed et al., 2018). Results presented in Figs. 6–7, and Tables 2–3 confirm the accuracy of the proposed method.

4.1. Convergence of MANA and HE-PFM

Fig. 8 shows the error versus number of iterations/terms required to achieve tolerance level, at nominal and 300% loading. Five decimal places have been set as the convergence tolerance. The MANA-PF method converged in 3 iterations for both loadings conditions, while HE-PFM takes 7 terms to converge. The proposed method offers quadratic convergence which is expected as it uses NR algorithm. Moreover, the proposed method requires around 60% less time than HE-PFM to achieve the same level of precision (see Fig. 9).

Although HE-PFM provides an early indicator of solution convergence/divergence, one possible issue with this method is the computational cost of locating roots. Calculating the Pade approximation makes sense only when combined with determining the roots of the denominator. Searching for the roots of high polynomials increases the computing load. Furthermore, if the number of power terms is very large, numerical errors in the Pade approximation computation may result in deceptive poles (Gonnet et al., 2013).

Table 2
Network losses comparison with four SSTs.

Stage-1 Overrating (%)	SST Location	SST rating (kVA)	Losses (kW) Ref (Guerra and Martinez-Velasco, 2017)	Losses (kW) Proposed	Losses (kW) HE-PFM
0	No-SST	-	202.67	202.67	202.67
5	3, 13, 22, 29	150, 144, 56, 150	181.59	180.99	181.05
10	3, 13, 22, 29	150, 144, 56, 150	176.89	176.54	176.41
15	3, 13, 22, 29	150, 144, 56, 150	174.49	174.36	174.28
20	3, 13, 22, 29	150, 144, 56, 150	173.23	172.96	172.98
25	3, 13, 22, 29	150, 144, 56, 150	171.12	170.01	170.00

Table 3
Network losses comparison with multiple SSTs.

No. of SSTs	Total installed rating (kVA)	SST (s) location	Losses (kW) Ref (Guerra and Martinez-Velasco, 2017)	Losses (kW) Proposed	Losses (kW) HE-PFM
0	-	-	202.67	202.67	202.67
1	500	29	165.83	165.12	165.83
2	600	13, 29	162.65	162.28	162.27
3	700	13, 28, 29	160.02	159.92	160.94
4	800	7, 13, 28, 29	158.21	158.01	158.05
5	900	7, 13, 28, 29, 31	155.90	155.47	155.45
6	1000	7, 13, 28, 29, 30, 31	153.82	153.37	153.39
7	1100	7, 13, 24, 28, 29, 30, 31	152.90	152.89	152.92
8	1200	6, 7, 13, 24, 28, 29, 30, 31	151.49	151.14	151.18
9	1300	3, 6, 7, 13, 24, 28, 29, 30, 31	150.61	150.53	150.54
10	1400	1, 3, 6, 7, 13, 24, 28, 29, 30, 31	150.52	150.38	150.41
11	1500	1, 3, 6, 7, 13, 22, 24, 28, 29, 30, 31	149.28	149.20	149.19

5. Conclusion

This paper developed the SST model for PF equations and implemented the NR algorithm with MANA formulation for PF solution. The accuracy of the proposed PF method is verified on the modified IEEE 33-bus DN with the existing solution in the literature. Different scenarios were simulated without SST and with multiple SSTs. Results suggest that

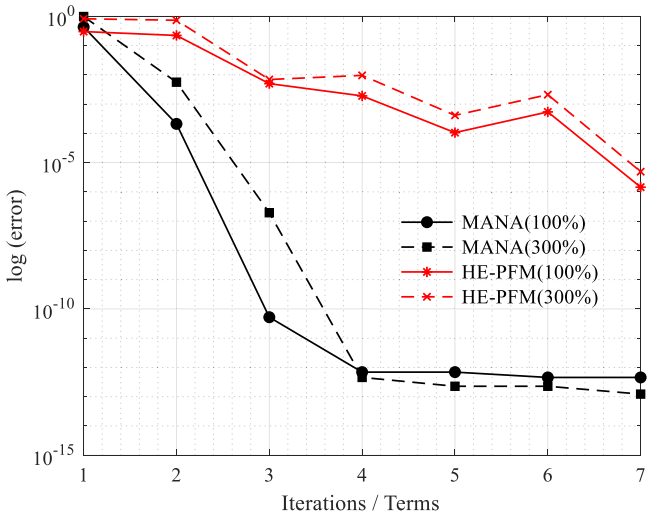

Fig. 8. Error versus iterations/terms.

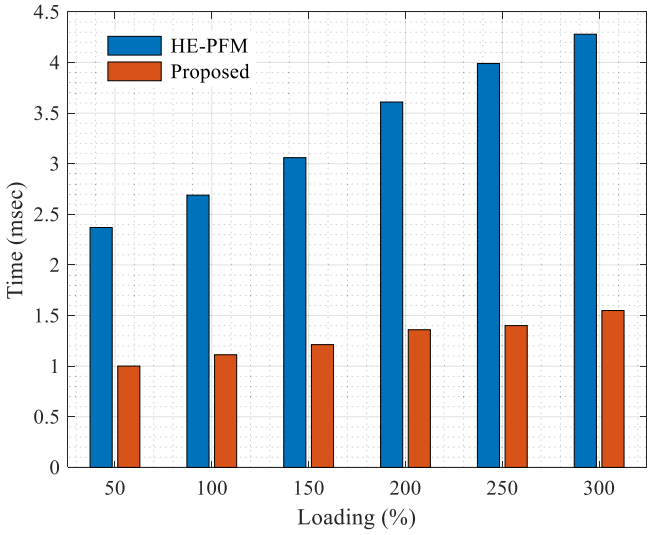

Fig. 9. Time comparison of MANA and HE-PFM at different loadings.

the network losses were reduced in all scenarios with SST integration, with single high rating SST being the best choice. Considering current technology, it may be more practical and feasible to install smaller units with lower ratings. This study found that SST can significantly impact the reduction of DN losses and/or improvement of voltage. The proposed MANA formulation is adoptable, and any arbitrary network configuration can be solved with the multiple SSTs integration. The MANA formulation offered faster convergence as compared to HE-PFM. Furthermore, MANA achieves the same level of accuracy as HE-PFM with approximately 60% less time required.

Declaration of Competing Interest

The authors declare no conflict of interest.

Data Availability

No data was used for the research described in the article.

Acknowledgements

Zahid Javid wishes to express his gratitude for the support received from the Hong Kong PhD Fellowship Scheme (HKPFS). Additionally, this work has been supported by the Hong Kong Research#Grant#Council under Grant number#15229421.

References

Cetindag, B., Kocar, I., Gueye, A., Karaagac, U., 2017. Modeling of step voltage regulators in multiphase load flow solution of distribution systems using newton's method and augmented nodal analysis. Electr. Power Compon. Syst. vol. 45 (15), 1667–1677.
Gonnet, P., Guttel, S., Trefethen, L.N., 2013. Robust Padé approximation via SVD. SIAM Rev. vol. 55 (1), 101–117.
Guerra, G., Martinez-Velasco, J.A., 2017. A solid state transformer model for power flow calculations. Int. J. Electr. Power Energy Syst. vol. 89, 40–51.
Javid, Z., Karaagac, U., Kocar, I., 2022. Improved Laplacian Matrix based power flow solver for DC distribution networks. Energy Rep. vol. 8, 528–537.
Javid, Z., Karaagac, U., Kocar, I., 2023. MANA formulation based load flow solution for DC distribution networks. IEEE Trans. Circuits Syst. II: Express Briefs.
Javid, Z., Xue, T., Karaagac, U., Kocar, I., 2023. Unified power flow solver for hybrid AC/DC distribution networks. IEEE Trans. Power Deliv.
Javid, Z., Xue, T., Karaagac, U., Kocar, I., 2023. Unified power flow solver for hybrid AC/DC distribution networks. IEEE Trans. Power Deliv.
Kocar, I., Mahseredjian, J., Karaagac, U., Soykan, G., Saad, O., 2013. Multiphase load-flow solution for large-scale distribution systems using MANA. IEEE Trans. Power Deliv. vol. 29 (2), 908–915.
W. Mcmurray, "Power converter circuits having a high frequency link," ed: Google Patents, 1970.
Mishra, D.K., et al., 2021. A review on solid-state transformer: a breakthrough technology for future smart distribution grids. Int. J. Electr. Power Energy Syst. vol. 133, 107255.
Mollik, M.S., et al., 2022. The advancement of solid-state transformer technology and its operation and control with power grids: a review. Electronics vol. 11 (17), 2648.
Nduka, O.S., Yu, Y., Pal, B.C., Okafor, E.N., 2019. A robust augmented nodal analysis approach to distribution network solution. IEEE Trans. Smart Grid vol. 11 (3), 2140–2150.
Qin, H., Kimball, J.W., 2010. A comparative efficiency study of silicon-based solid state transformers. 2010 IEEE Energy Conversion Congress and Exposition. IEEE, pp. 1458–1463.
Rao, S., Feng, Y., Tylavsky, D.J., Subramanian, M.K., 2015. The holomorphic embedding method applied to the power-flow problem. IEEE Trans. Power Syst. vol. 31 (5), 3816–3828.
Syed, I., Khadkikar, V., Zeineldin, H.H., 2018. Loss reduction in radial distribution networks using a solid-state transformer. IEEE Trans. Ind. Appl. vol. 54 (5), 5474–5482.
Trias, A., 2012. The holomorphic embedding load flow method. 2012 IEEE Power and Energy Society General Meeting. IEEE, pp. 1–8.
Wedepohl, L., Jackson, L., 2002. Modified nodal analysis: an essential addition to electrical circuit theory and analysis. Eng. Sci. Educ. J. vol. 11 (3), 84–92.
Zhuang, Y., et al., 2021. A Multiport DC solid-state transformer for MVDC integration interface of multiple distributed energy sources and DC loads in distribution network. IEEE Trans. Power Electron. vol. 37 (2), 2283–2296.